

1 **Assessment of variability of TEC and improvement of**  
2 **performance of the IRI model over Ethiopia during**  
3 **the high solar activity phase**

4 Yekoye Asmare Tariku

5 Department of Space Science and Research Application Development, Ethiopian Space  
6 Science and Technology Institute, Addis Ababa, Ethiopia

7  
8 \* Corresponding author. Tel. +251912799754

9 *Email\_address:yekoye2002@gmail.com (Yekoye Asmare)*

10 **Abstract**

11 This paper discusses the monthly and seasonal variation of the total electron content (TEC) and  
12 the improvement of performance of the IRI model in estimating TEC over Ethiopia during the  
13 solar maximum (2013-2016) phase employing GPS TEC data inferred from the GPS receivers  
14 installed at different regions of Ethiopia. **The results reveal that, in the year 2013-2016, the**  
15 **highest peak measured seasonal diurnal VTEC value is observed in the March equinox in**  
16 **2015 over Arba Minch station.** Moreover, both the arithmetic mean measured and modeled  
17 VTEC values, generally, show maximum and minimum values in the equinoctial and June  
18 solstice months, respectively in 2014-2015. **However, in 2013, the minimum and maximum**  
19 **arithmetic mean measured values are observed in the March equinox and December**  
20 **solstice, respectively.** The results also show that, even though overestimation of the modeled  
21 VTEC has been observed on most of the hours, all versions of the model are generally good to

22 estimate both the monthly and seasonal diurnal hourly VTEC values, especially in the early  
23 morning hours (00:00-03:00 UT or 03:00-06:00 LT). **It has also been shown that the IRI 2007**  
24 **and IRI 2012 versions are generally better when the solar activity decreases; while, IRI**  
25 **2016 is better when the solar activity increases to capture the GPS VTEC values. In**  
26 **addition, the IRI 2012 version with IRI2001 option for the topside electron density shows**  
27 **the highest overestimation of the VTEC as compared to the other options.** All versions of the  
28 model do not also able to capture the effects resulting from storm.

29 **Key words:** GPS-VTEC; IRI- VTEC; GPS signal, solar maximum

30

## 31 **1. Introduction**

32 The energy transferred from the sun causes atoms and molecules existing in the  
33 atmosphere to undergo chemical reactions and become ionized (Kelley, 2009). This ionized and  
34 conductive region of Earth's atmosphere, extending from about 50 to 1000 km and possessing  
35 free electrons and positive ions generally in equal numbers in a medium that is electrically  
36 neutral, is termed as ionosphere. The existence of these ions (plasma) in the ionosphere results in  
37 the possibility of radio communications over large distance by making use of one or more  
38 ionospheric reflections (Hunsucker and Hargreaves, 2003).

39 On the other hand, the ionosphere affects the electromagnetic waves that pass through it  
40 by inducing additional transmission time delay (Gao and Liu, 2002). Because of its dispersive  
41 character, electromagnetic signals (such as GPS signals) experience time delay (modulated  
42 codes) and advance (carrier phase) as they propagate through the ionosphere. This delay is  
43 directly proportional to the integral number of electrons in a unit cross-sectional area (usually  
44 referred to as total electron content, TEC) along the signal path extending from the satellite to the

45 receiver on the ground, and inversely proportional to the square of the frequency of propagation  
46 (Hofmann-Wellenhof et al., 1992; Misra and Enge, 2006). The dispersive ionosphere introduces  
47 a time delay in the 1.57542 GHz (L1) and 1.22760 GHz (L2) simultaneous transmissions from  
48 GPS satellites orbiting at 20,200 km (Hansen et al., 2000). The relative ionospheric delay of the  
49 two signals is proportional to the TEC. Time delay measurements of L1 and L2 frequencies can,  
50 therefore, be converted to TEC along the ray path from the receiver to the satellite (Lanyi and  
51 Roth, 1988). The GPS signals traverses the ionosphere carrying signatures of the dynamic  
52 medium and thus offers opportunities for ionospheric research. As a result, global and regional  
53 maps of ionospheric TEC can be produced using data from the worldwide network of the  
54 International GPS Service (Lanyi and Roth, 1988). The availability of TEC measurements is also  
55 important to the development of ionospheric models such as the International Reference  
56 Ionosphere, IRI (Bilitza, 2001). The International Reference Ionosphere (IRI) is an international  
57 project sponsored by the Committee on Space Research (COSPAR) and the International Union  
58 on Radio Science (URSI).

59 Using the GPS satellites and the IRI model, there have been so far several researches  
60 conducted globally in connection with the TEC variability and performance of the model over  
61 equatorial and low latitude regions, especially using IRI 2007 and IRI 2012 versions (e.g. Ezquer  
62 et al., 2014; Luhr and Xiong, 2010; Nigussie et al., 2013; Sethi et al., 2011; Olwendo et al.,  
63 2012a; Olwendo et al., 2012b). Nigussie et al., 2013, for instance, reported that IRI 2007 model  
64 overestimates the VTEC values over the East African equatorial regions. Using IRI 2007, Sethi  
65 et al., 2011, also showed that using IRI 2007 model with IRI 2001 option for the topside electron  
66 density highly overestimates the VTEC in all seasons and times over low and equatorial Indian  
67 regions. Olwendo et al. (2012a) also noted that seasonal average IRI 2007 TEC values were

68 higher than the GPS-TEC data for the period of 2009-2011 over different regions in Kenya. In  
69 addition, Olwendo et al. (2012b) reported that the IRI 2007 TEC is too high for all seasons  
70 except for the March equinox (where there seems to be good agreement between observation and  
71 model) during the lowest solar activity phase (2009-2010). Ezquer et al. (2014), using IRI 2012,  
72 noted that IRI 2012 predictions show significant deviations from experimental values during the  
73 period of 2008-2009 for a station placed at the southern crest of the equatorial anomaly in the  
74 American region. The report of Kumar (2016) on the validation of the IRI 2012 models for the  
75 global equatorial region also showed that the IRI 2012 model generally overestimated the  
76 observed VTEC over equatorial regions during the solar minimum year (2009) and solar  
77 maximum (2012) phases. Asmare et al. (2014) and Tariku, 2015a and Tariku, 2015b also  
78 attempted to see patterns in both the measured and modeled VTEC variations during the low and  
79 high solar activity phases employing different GPS stations and IRI 2012 model at various  
80 regions of Ethiopia. Asmare et al. (2014), for instance, showed that the IRI 2012 model entirely  
81 overestimates both monthly and seasonal VTEC values during phases of low solar activity. In  
82 addition, the model performance in estimating diurnal VTEC variations was found to be better  
83 during low solar activity phases than during high solar activity phases. In addition, the highest  
84 and the lowest values of the VTEC are observed in the equinoctial and the June solstice months,  
85 respectively during both the low and high solar activity phases. Abdu et al. (1996); Kakinami et  
86 al. (2012); Kumar et al. (2015) also attempted to describe the model's capacity to estimate the  
87 TEC using different versions of the model. **However, different findings show that the**  
88 **assessment of the improvement of the model performance from the relatively old to new**  
89 **versions for TEC estimation purpose in long lasting period is lacking over low latitude and**  
90 **equatorial regions, such as Ethiopia though the model has been steadily improved and**

91 arrived at the most recent version (IRI 2016). Hence, for a better improvement of the IRI  
92 model in estimating the variation of TEC, its performance has to be continuously tested,  
93 especially over the equatorial and low latitude regions where the dynamics of the  
94 ionosphere is very complex. In addition, there are few researches conducted to test the  
95 performance of the IRI 2016 model over the region. The model includes some new features  
96 that are supposed to enhance its performance in estimating different ionospheric  
97 parameters. For instance, the two new model options for the F2-peak height  $hmF2$  and a  
98 better representation of topside ion densities at very low and high solar activities enable the  
99 model in estimating  $hmf2$  directly and no longer through its relationship to the propagation  
100 factor  $M(3000)F2$ . As a result, the new model options make the IRI 2016 model estimate  
101 evening peaks that was not possible in the old versions.

102 Thus, this study is mainly important to observe the TEC variation and the improvement of  
103 performance of the IRI model in estimating the TEC variation over low latitude African regions  
104 during the high solar activity phase (2013-2016) employing the GPS VTEC data inferred from  
105 different regions of Ethiopia. To observe the TEC variation and improvement of performance of  
106 the IRI model in estimating the TEC variation, the latest versions (IRI 2007, IRI 2012 and IRI  
107 2016) during the solar maximum phase have been considered. The prediction performance of the  
108 model has been tested by comparing the modeled TEC values with the GPS-TEC values  
109 recorded in the receivers.

110

## 111 **2. Data description and analysis method**

112

### 113 *2.1. TEC from dual frequency GPS receiver*

114 As different studies (such as Ciraolo et al., 2007; Mannucci et al., 1998) show the GPS  
 115 measurements are used to estimate the TEC along a ray path between a GPS satellite and  
 116 receiver on the ground. These GPS measurements can be recorded using either single or dual  
 117 frequency GPS receivers. However, to eliminate ionospheric errors in the estimation of TEC dual  
 118 frequency receivers are better (Klobuchar, et al., 1996). Moreover, by computing the  
 119 differential phases of the code and carrier phase measurements, dual frequency GPS receivers  
 120 can provide integral information about the ionosphere and plasma sphere (Ciraolo et al., 2007;  
 121 Nahavandchi and Soltanpour, 2008). Hence, in this paper, the GPS-TEC data have been obtained  
 122 from dual frequency receiver using pseudo-range and carrier phase measurements. The TEC  
 123 inferred from the pseudo-range (P) measurement is given by:

$$124 \quad TEC_P = \frac{1}{40.3} \left[ \frac{f_1^2 f_2^2}{f_1^2 - f_2^2} \right] (P_2 - P_1). \quad (1)$$

125 Similarly, the TEC from carrier phase measurement ( $\Phi$ ) is given as

$$126 \quad TEC_\Phi = \frac{1}{40.3} \left[ \frac{f_1^2 f_2^2}{f_1^2 - f_2^2} \right] (\Phi_1 - \Phi_2), \quad (2)$$

127 where  $f_1$  and  $f_2$  can be related with the fundamental frequency,  $f_o = 10.23MHz$

$$128 \quad \begin{aligned} f_1 &= 154f_o = 1575.42MHz, \\ f_2 &= 120f_o = 1227.60MHz. \end{aligned} \quad (3)$$

129 As shown above, by cross correlating the  $f_1$  and  $f_2$  modulated carrier signals which are  
 130 generally assumed to travel along the same path through the ionosphere, the GPS receiver  
 131 obtains the time delay of the code and the carrier phase difference. **The TEC obtained from  
 132 code pseudo-range measurements is free of ambiguity, but with relatively much noise. On**

133 the other hand, the TEC obtained from carrier phase measurements has relatively less  
134 noise, but it is ambiguous. Thus, linearly combining both code pseudo-range and carrier  
135 phase measurements for the same satellite pass is believed to increase the accuracy of TEC  
136 (Ciraolo et al., 2007; Gao and Liu, 2002; Klobuchar et al., 1996). This resultant absolute  
137 TEC is the GPS-derived STEC along the signal from the satellite to the receiver on the  
138 ground. To better characterize the TEC over a given receiver position and see the overall  
139 ionization of the Earth's ionosphere, the slant TEC (STEC) must be converted into equivalent  
140 vertical TEC (VTEC) at the mean ionospheric height,  $h_m=350$  km (Mannucci et al., 1998;  
141 Norsuzila et al., 2008, 2009). Hence, the relationship between STEC and VTEC in terms of the  
142 zenith angle  $\chi'$  at the Ionospheric Piercing Point (IPP) and the zenith angle  $\chi$  at the receiver  
143 position can be given by:

$$144 \quad VTEC = STEC(\cos \chi'), \quad (4)$$

145 where,

$$146 \quad \chi' = \arcsin\left[\frac{R_e}{R_e + h_m} \sin \chi\right]. \quad (5)$$

147 Substituting equation (5) into equation (4) and rearranging, we get

$$148 \quad VTEC = STEC \left\{ \cos \left[ \arcsin \left( \frac{R_e}{R_e + h_m} \sin \chi \right) \right] \right\}. \quad (6)$$

149 Here,  $R_e$  is the radius of the Earth in kilometers.

150

## 151 2.2. TEC from the International Reference Ionosphere (IRI) model

152

153           The International Reference Ionosphere (IRI) is an international empirical standard  
154 model used for the specification of ionospheric parameters. The model provides average values  
155 of electron density, electron content, electron and ion temperature, and ion composition as a  
156 function of height, location, local time, and sunspot number for magnetically quiet conditions  
157 (Bilitza, 2001; Bilitza et al., 2014; Bilitza et al., 2017). To enhance the capacity of the model,  
158 improvements have been made through the ingestion of all worldwide available data from  
159 ground-based as well as satellite observations. As a result, a new version of the model (IRI 2016)  
160 has been released in 2017 by incorporating some new input parameters that are supposed to  
161 increase its capacity. The IRI 2016 model includes two new model options for the F2-peak  
162 height  $hmF2$  and a better representation of topside ion densities at very low and high solar  
163 activities. The two new options are used in modeling  $hmf2$  directly and no longer through its  
164 relationship to the propagation factor  $M(3000)F2$ . Thus, the new model options enable the IRI  
165 2016 model to predict evening peaks that was not possible in the old versions. In addition, the  
166 improvement of the ion composition model in the topside ionosphere can lower the transition  
167 height from close to 1000 km down to almost 600 km in the new version of the model. A number  
168 of smaller changes have also been made concerning the use of solar indices and the speed-up of  
169 the computer program (Bilitza et al., 2017). For a given location, time and date, like the previous  
170 versions of the model, the IRI-2016 model provides the monthly averages of ionospheric  
171 parameters (such as TEC) in the altitude range from about 50–2000 km (Bilitza et al., 2017;  
172 <http://IRImodel.org>). For more information, see the model web site  
173 (<http://omniweb.gsfc.nasa.gov/vitmo/iri-vitmo.html>) that was accessed for the period of 25-  
174 30/01/2018.

175



176 2.3. *Data sources and method of analysis*

177 The data required for both the experimental and model were obtained from Ethiopian **sites**  
178 shown in Figure 1 during the solar maximum (2013-2016) phase. Table 1 also shows the GPS  
179 receiver locations used for the study. The raw GPS data for the described station were obtained  
180 from the University NAVSTAR Consortium (UNAVCO web site, <http://www.unavco.org/>). The  
181 data gained from this web site have two forms: observation and navigation data in which both of  
182 them are zipped. To use the data for the desired purpose, the GG software (GPS-TEC calibrating  
183 software) was used to process the required data in five minutes interval and an elevation cut-off  
184  $10^\circ$ .

185 To get the required results, the corresponding modeled VTEC values were inferred from the  
186 latest versions of the model (IRI 2007, IRI 2012 and IRI 2016) that include some latest input  
187 parameters which are supposed to improve the capacity of the model in estimating ionospheric  
188 parameters. The online IRI versions of the model were obtained from  
189 <http://omniweb.gsfc.nasa.vitmo.html>. To get the VTEC values, the year, date, month, location,  
190 the hour profile, the upper boundary altitude (2000 km), daily sunspot number and **F10.7 cm**  
191 **flux**, topside electron density options (NeQuick, IRI01, IRI2001), CCIR for F peak model have  
192 been used. Here, the IRI 2012 version has been used with NeQuick, IRI01 and IRI2001 options  
193 for the topside electron density in the year 2013-2014. However, in the year 2015-2016, all  
194 versions of the model have been used with NeQuick option for the topside electron density.

195 In order to observe the pattern of the hour-to-hour variability of VTEC, the mean monthly  
196 and seasonal hourly GPS TEC and the corresponding IRI TEC data have been used during the  
197 period of 2013-2016. To see the monthly and seasonal arithmetic mean VTEC variation and the  
198 model performance, the hour-to-hour measured and modeled VTEC values have been

199 correspondingly added and averaged for the whole days in each month and season. The seasons  
200 could be classified as December solstice (November, December and January), March equinox  
201 (February, March and April), June solstice (May, June and July) and September equinox  
202 (August, September and October). For a better understanding on the performance of the model,  
203 the absolute differences between the monthly and seasonal GPS VTEC and the corresponding  
204 IRI VTEC values have been determined. The differences have been calculated by subtracting the  
205 experimental VTEC values from the model. In order to clearly see the validation of the model,  
206 the absolute differences between the IRI VTEC and GPS VTEC in all the monthly and seasonal  
207 variations were determined. In addition, the percentage differences between the IRI VTEC and  
208 GPS VTEC for the arithmetic monthly and seasonal VTEC variations have also been determined.

### 209 **3. Results and discussion**

#### 210 *3.1. Diurnal monthly and seasonal variation of VTEC and performance of the IRI model*

211

212 **The results of the variations of the monthly and seasonal hourly VTEC are displayed in**  
213 **Figs. 2-7. As observed in the figures, both the measured and modeled VTEC values start**  
214 **decreasing in the nighttime hours and become minimum after midnight hours (on average**  
215 **at 03:00 UT or 06:00 LT) and start increasing again to attain their peak values in the time**  
216 **interval of about 09:00-13:00 UT or 12:00-16:00 LT). Moreover, in some hours, the modeled**  
217 **VTEC values (in all versions) are in a good agreement with the measured (GPS VTEC) values,**  
218 **especially in the nighttime hours (00:00-03:00 UT or 03:00-06:00 LT). On the other hand, all**  
219 **versions of the model tend to underestimate the VTEC values during the daytime hours (09:00-**  
220 **13:00 UT or 12:00-16:00 LT). Overestimations are also observed, especially in using IRI**  
221 **2001 option for IRI 2012 model in 2013-2014 (see Figs. 4 and 5) and using IRI 2016 model**

222 **in 2016 (see Fig. 7). In the year 2013-2016, the highest underestimation (by about 30 TECU)**  
223 **and highest overestimation (by about 20 TECU) are observed in the March equinox in 2015**  
224 **(using IRI 2016 model) and June solstice in 2014 (using IRI 2012 model with IRI2001**  
225 **option), respectively at about 12:00 UT (15:00 LT). However, the IRI 2007 and IRI 2012**  
226 **are generally better to capture the VTEC values as the solar activity decreases; while, IRI**  
227 **2016 version is generally better when the solar activity increases. Moreover, the IRI 2012**  
228 **version with NeQuick and IRI01 options gives hourly VTEC variation having closer hourly**  
229 **VTEC values (see Figs. 4 and 5). The mismodelings observed in both cases may be due to the**  
230 **difference in the model and experimental slab-thickness as noted by different findings (e.g.**  
231 **Nigussie et al., 2013; Rios et al., 2007). For instance, Rios et al. (2007) using the IRI 2001**  
232 **model, showed that IRI predicted slab thickness is higher than the measured values except**  
233 **between (10:00-14:00 LT) which can attribute to VTEC fluctuations in similar trend. This is**  
234 **almost consistent with the result determined in this work. Using IRI 2007 model, Nigussie et al.**  
235 **(2013) also suggested similar possible reason for the discrepancy between the model and the**  
236 **experimental VTEC values. It could also be resulting from poor estimation of the hmF2 and foF2**  
237 **from the coefficients, which in turn may result in poor estimation of VTEC by the IRI model**  
238 **(e.g. Chakraborty et al., 2014; Kumar et al, 2015). The underestimation of the IRI VTEC values**  
239 **by the GPS VTEC values may also attribute to the enhancement of the plasmaspheric electron**  
240 **content above 2000 km during the daytime hours (Coisson et al., 2008; Aggarwal, 2011;**  
241 **Venkatesh et al., 2011).**

242 Moreover, the maximum peak of both the measured and modeled VTEC values are  
243 generally observed in the equinoctial months; while, the minimum peak values are observed in  
244 the June solstice months (see Fig. 2-7). For instance, over Arba Minch station (see Figs. 2 and 3),

245 the highest and lowest peak measured monthly VTEC values of about 80 and 40 TECU are  
246 observed in March and July, respectively in 2015. Similarly, the highest and lowest peak  
247 modeled monthly VTEC values of about 55 and 41 TECU are observed in April and July,  
248 respectively in using IRI 2007 model with NeQuick option for the topside electron density. In  
249 addition, the highest and lowest peak measured seasonal VTEC values of are observed in the  
250 March equinox and June solstice, respectively in 2015. The highest and lowest peak modeled  
251 seasonal VTEC values of about 54 and 43 TECU are also observed in the March equinox and  
252 June solstice, respectively when using IRI 2007 model with NeQuick option for the topside  
253 electron density over Arba Minch station (see Fig. 6). In addition, in using IRI 2012 model with  
254 IRI2001 option for the topside electron density, the highest and lowest peak measured seasonal  
255 VTEC values of about 70 and 40 TECU are observed in the March equinox and June solstice,  
256 respectively over Ambo station in 2014. Similarly, the highest and lowest peak modeled seasonal  
257 VTEC values of about 74 and 60 TECU are observed in the March equinox and June solstice,  
258 respectively in 2014 when using the same version of the model (IRI 2012) with IRI2001 option  
259 (see Fig. 5). **The overall results show that, in the year 2013-2016, the highest peak measured**  
260 **VTEC values of about 80 TECU is observed in the March equinox in 2015.**

261 It is known that, in general, electron population in the ionosphere is mainly controlled by  
262 solar **photoionization** and recombination processes (Wu et al., 2004). Thus, for the equinoctial  
263 months, as the subsolar point is around the equator where the **eastward** electrojet associated  
264 electric field is often largest, it would be speculated that the peak photoelectron abundance and  
265 intense eastward electric field will be set up in the described region. On the contrary, for solstice  
266 months photoelectrons at the equator decrease as the **subsolar** point moves to higher latitudes.  
267 Moreover, the change of direction of neutral wind may account for the highest VTEC values in

268 the equinoctial months and lowest values in the June solstice months. A meridional component  
269 of neutral wind blows from the summer to the winter hemisphere that is able to reduce the  
270 ionization crest value during summer solstice as it blows in an opposite direction to the plasma  
271 diffusion process originating from the magnetic equator. Thus, in equinoxes meridional winds  
272 blowing from the equator to polar regions may attribute to a high ionization crest value. Hence, a  
273 seasonal effect on the crest should be expected with the crest maximum at the equinoxes and  
274 minimum in the summer season or June solstice (Bhuyan and Borah, 2007; Wu et al., 2004),  
275 which is consistent with the result of this work.

276

### 277 *3.2. Arithmetic mean of monthly and seasonal variations of VTEC and performance of the IRI* 278 *model*

279 **The results of the arithmetic mean monthly and seasonal VTEC variations are given in**  
280 **Figures 8-11.** The results show that both the measured and the modeled arithmetic mean VTEC  
281 have generally the highest and lowest values in the equinoctial and June solstice months. For  
282 example, the highest and lowest measured arithmetic mean monthly VTEC values of about 38  
283 and 18 TECU are observed in April and July, respectively in 2014 over Ambo station (see the  
284 left top panel of Fig. 9). The seasonal measured arithmetic mean VTEC variation also shows the  
285 highest and lowest values of about 37 and 21 TECU in the March equinox and June solstice,  
286 respectively in 2014 (see the left bottom panel of Fig. 9). In addition, the highest and lowest  
287 seasonal measured VTEC values of about 36 and 23 TECU are observed in the March equinox  
288 and June solstice, respectively over Arba Minch station in 2015. The highest and lowest seasonal  
289 modeled arithmetic mean VTEC values of about 32 and 24 TECU are also observed in the March  
290 equinox and June solstice, respectively when using IRI 2007 version (see the left bottom panels

291 of Fig. 10). On the other hand, the highest and lowest measured monthly VTEC values are  
292 observed in November and February, respectively in 2013. Similarly, the highest and lowest  
293 measured seasonal VTEC values are observed in the December solstice and March equinox,  
294 respectively (see the left top and bottom panels of Fig. 8). But, the highest and lowest modeled  
295 arithmetic mean seasonal VTEC values are observed in the March equinox and June,  
296 respectively in 2013 when using IRI 2001 option for the topside electron density (see the left top  
297 panel of Fig. 8). **In the year 2013-2014, using the IRI 2012 model with IRI2001 option for the**  
298 **topside electron density shows the highest overestimation as compared to NeQuick and**  
299 **IRI01 options. As shown in the Figures (see the right top and bottom panels of Figs. 8 and**  
300 **9), the highest monthly and seasonal overestimations are observed in July (by about 130%)**  
301 **and the June solstice (by about 100%) in 2014. On the other hand, the IRI 2012 version**  
302 **with NeQuick and IRI01 options relatively gives VTEC having closer values (see Figs 8 and**  
303 **9). Moreover, the IRI 2016 version shows overestimation of the VTEC as compared to**  
304 **others (IRI 2007 and IRI 2012), especially when the solar activity decreases.** For instance,  
305 the highest monthly and seasonal deviations of about 25% and 20% are observed between the  
306 modeled and corresponding measured values in September and the June solstice, respectively  
307 when IRI 2016 version is used (see the top and bottom right panels of Fig. 10).

308

### 309 *3.3 Storm Time VTEC variation and performance of the IRI model*

310 To see the VTEC variation and performance of the IRI model during storm time condition, the  
311 magnetic storm day (with **Dst index maximum incursion of about -222nT**) which occurred on  
312 March 17, 2015 as observed over Arba Minch station was considered (see **Fig. 12**). **As shown in**  
313 **the figure (see Figure 12), the storm started with a sudden impulse/sudden storm**

314 **commencement at 04:45 UTC on 17 March. This sudden impulse represents a sharp change**  
315 **in how the solar wind was driving space weather conditions at the Earth, including space**  
316 **weather conditions in the ionosphere. Thus, the sudden impulse acts as a shock to the**  
317 **magnetosphere-ionosphere system. As a result, to better see the effect of the storm on the**  
318 **VTEC, the patterns of the VTEC fluctuations during conditions prior to the onset of the**  
319 **storm (16/03/2015) and the recovery phase (18/03/2015) of the storm were also considered.**  
320 As shown in Fig. 13, the GPS-VTEC values show significant fluctuation that indicates the  
321 occurrence of storm. On the other hand, the model VTEC values (IRI 2007, IRI 2012 and IRI  
322 2016 VTEC) don't show any change when the storm model is "on" and "off" (see Figs.13a-13c  
323 and Figs.13d-13f). As shown in the figures, the mode VTEC values in all the three days follow  
324 almost similar pattern; they generally tend to underestimate the VTEC values (mostly after 08:00  
325 UT or 11:00 LT) and remain smooth during the storm. This shows that the model does not  
326 respond to the effects resulting from storm. **The IRI 2016 VTEC values are also smaller than**  
327 **those of the IRI 2007 and IRI 2012 VTEC values during conditions prior to the onset of the**  
328 **storm, main and recovery phase of the storm.** In addition, enhancement of GPS TEC is  
329 observed as we proceed from the initial to the recovery phase of the storm. As shown in the  
330 figure, a peak VTEC value of about 65 TECU being observed during conditions prior to the  
331 onset of the storm increases to about 75 TECU in the recovery phase of the storm. This may be  
332 resulting from particle transport and the prompt penetration of high latitude electric fields  
333 (PPEFs) to lower latitude which travel equator ward with high velocities during the storm (Malik  
334 et al., 2010; Sobral et al., 2001; Tsurutani et al., 2004). **As the findings show, the dayside**  
335 **ionospheric storms resulting from PPEFs are characterized by transport of near-equatorial**  
336 **plasma to higher altitudes and latitudes, producing a giant plasma fountain. Hence, if the**

337 **electric field penetrates into the dayside equatorial ionosphere, the plasma is convected**  
338 **toward higher altitudes, forming a giant plasma fountain. At these higher altitudes, the**  
339 **recombination rates are longer than for lower altitudes. On the other hand, solar**  
340 **photoionization at lower altitudes simultaneously continues to occur. This photoionization**  
341 **process will replace the uplifted plasma resulting in an overall increment of TEC.**

342

#### 343 4. Conclusions

344 Because of the unique geometry of the geomagnetic field near the magnetic equator and low  
345 latitude regions (such as Ethiopia), the signal propagation system through the ionosphere is  
346 largely affected by the accumulation of electrons (TEC). Hence, in this study, the VTEC  
347 variation and the improvement of performance of the IRI model over the equatorial and low  
348 latitude regions has been studied employing the GPS and IRI techniques during the period of  
349 2013-2016. **The results reveal that, in the year 2013-2016, the maximum seasonal arithmetic**  
350 **mean measured VTEC values are observed in the March equinox except in 2013 in which**  
351 **the minimum and maximum being observed in the March equinox and December solstice,**  
352 **respectively.** In addition, though overestimation of the modeled VTEC has been observed on  
353 most of the hours, the model is generally good to estimate the diurnal hourly VTEC values  
354 mostly just after midnight hours (00:00-03:00 UT or 03:00-06:00 LT). It has also been shown  
355 that the IRI 2012 version of the model generally overestimates both the arithmetic mean of the  
356 monthly and seasonal hourly VTEC values, with the highest overestimation being observed in  
357 using IRI2001 option in 2013-2014. In general, the model does not show good improvements  
358 from version IRI 2007 to IRI 2016 in the TEC estimation over equatorial and low latitude  
359 regions. **However, the IRI 2007 and IRI 2012 versions are generally better to respond to the**



360 **decrement of the VTEC values when the solar activity decreases; while IRI 2016 version is**  
361 **generally better to capture the measured VTEC values when the solar activity increases.**  
362 **Moreover,** all versions of the model do not respond to the effects resulting from storm. Hence,  
363 further improvements have to be made on the model for the betterment of its performance in  
364 estimating the VTEC over the equatorial and low latitude regions.

#### 365 **Author contribution**

366 All the required issues for the manuscript are prepared by the corresponding author, Yekoye

#### 367 **Competing interests**

368 The corresponding author declares that he has no conflict of interest.

#### 369 **Acknowledgements**

370

371 The data of daily sunspot number, GPS, Dst index and IRI model for this paper are freely  
372 available at: <http://www.sidc.be/sunspot-data/>, <http://facility.unavco.org/data/dai2/app/dai2..>,  
373 [http://wdc.kugi.kyoto-u.ac.jp/dst\\_final/201401/index.html](http://wdc.kugi.kyoto-u.ac.jp/dst_final/201401/index.html) and  
374 ([http://omniweb.gsfc.nasa.gov/vitmo/iri\\_vitmo.html](http://omniweb.gsfc.nasa.gov/vitmo/iri_vitmo.html)), respectively. Hence, the author is very  
375 grateful to UNAVCO, NOAA, World Data Center (Kyoto University) and NASA for donating  
376 their free GPS, daily sunspot number, Dst index and online IRI model data, respectively.

377

#### 378 **References**

379

380 Abdu, M.A., Batista, I.S., Souza JR. (1996); An overview of IRI-observational data  
381 comparison in American (Brazilian) sector low latitude ionosphere. Adv Space  
382 Res 18(6):13-22.

383 Aggarwal, M. (2011); TEC variability near northern EIA crest and comparison with IRI model,  
384 Adv. Space Res., 48(7), 1221–1231, doi:10.1016/j. asr.2011.05.037

385 Asmare Y., Tsgaye, K., Melssew, N. (2014); Validation of IRI-2012 TEC model over  
386 Ethiopia during solar minimum (2009) and solar maximum (2013) phases. Adv  
387 Space Res, 1582-1594, <http://dx.doi.org/10.1016/j.asr.2014.02.017>.

388 Bhuyan, P.K., Borah,R.R. (2007); TEC derived from GPS net work in India and comparison  
389 with IRI. Advances in Space Research: The Official Journal of the Committee on Space  
390 Research (COSPAR) 39, 830-840.

391 Bilitza, D. (2001); International reference ionosphere 2000. Radio Sci. 36(2), 261-275.

392 Bilitza, D., D. Altadill, Y. Zhang, C. Mertens, V. Truhlik, P. Richards, L. McKinnell, and  
393 B. Bodo Reinisch, (2014); The International Reference Ionosphere 2012 – a model of  
394 international collaboration, J. Space Weather Space *Clim.*, 4, A07, DOI:  
395 10.1051/swsc/2014004

396 Bilitza1, D, D. Altadill, V. Truhlik, V. Shubin, I. Galkin, B. Reinisch, X. Huang (2017);  
397 International Reference Ionosphere 2016: from ionospheric climate to real-time weather  
398 predictions, Space Weather, DOI: 10.1002/2016SW001593.

399 Chakraborty,M., Kumar, S., Kumar, B., Guha, A.(2017); Latitudinal characteristics of GPS  
400 derived ionospheric TEC: a comparative study with IRI 2012 model, Annals of  
401 Geophysics, 57 (5), A0539; doi: 10.4401/ag-6438.

402 Ciraolo, L., F. Azpilicueta, C. Brunini, Meza, A. and S. M. Radicella (2007); Calibration errors  
403 on experimental slant total electron content (TEC) determined with GPS, *J., Geodesy*, 81,  
404 111–120

405 Coisson P., S. M. Radicella, L. Ciralo, R. Leitinger, and B. Nava (2008); Global validation of

406 IRI TEC for high and medium solar activity conditions, *Adv. Space Res.*, 42, 770–775.

407 Ezquer, R.G., López, J.L., Scidá, L.A., Cabrera, M.A., Zolesi, B., Bianchi, C., Pezzopane M.,  
408 Zuccheretti, E., Mosert, M. (2014); Behaviour of ionospheric magnitudes of F2 region over  
409 Tucumán during a deep solar minimum and comparison with the IRI 2012 model  
410 predictions. *J. Atmos. Sol-Terr. Phys.* 107:89-98.

411 Gao, Y., Liu, Z.Z. (2002); Precise ionospheric modeling using regional GPS network data, *Journal*  
412 *of Global Positioning system*, vol. 1, No. 1:18-24.

413 Hansen, A., Blanch, J., T. Walter, T. (2000); Ionospheric correction analysis for WAAS quiet and  
414 stormy, in *Proceedings of the 13<sup>th</sup> International Technical Meeting of the Satellite Division*  
415 *of The Institute of Navigation ION GPS*, Salt Lake City, Utah, 19-22.

416 Hofmann-Wellenhof, B., Lichtenegger, H., Collins, J. (1992); *Global Positioning System Theory*  
417 *and Practice*. Springer-Verlag Wien, New York.

418 Hunsucker, R.D. and Hargreaves, R.D. (2003); *The high-latitude ionosphere and its effects on*  
419 *radio propagation*, Cambridge Univ. Press, UK.

420 Kakinami, Y., Liu, J.Y., Tsai, L.C. (2012); A comparison of a model using the FORMOSAT-  
421 3/COSMIC data with the IRI model. *Earth, Planets, Space*, 64:545-551.

422 Kelley, M.C. (2009); *The Earth's Ionosphere: Plasma Physics and Electrodynamics*,  
423 *Second Edition*. Elsevier Inc., New York.

424 Kumar, S., Tan, E., Murti. D. (2015); Impacts of solar activity on performance of the IRI-2012  
425 model predictions from low to mid latitudes. *Earth, Planets, Space*, 67:42.  
426 doi:10.1186/s40623-015-0205-3

427 Kumar, S. (2016); Performance of IRI-2012 model during a deep solar minimum and a  
428 maximum year over global equatorial regions, *J. Geophys. Res., Space Physics*, 121,

429 doi:10.1002/2015JA022269.

430 Klobuchar, J.A., Parkinson, B.W., Spilker, J.J. (1996); Ionospheric effects on GPS, in: Global  
431 Positioning System: Theory and Applications, American Institute of Aeronautics and  
432 Astronautics, Washington, DC.

433 Lanyi, G.E. and Roth, T. (1988); A Comparison of Mapped and Measured Total Ionospheric  
434 Electron Content Using Global Positioning System and Beacon Satellite Observations.  
435 Radio Science, Vol. 23, No. 4, pp. 483-492.

436 Luhr, H., Xiong, C. (2010); IRI-2007 model overestimates electron density during the 23/24  
437 solar minimum, Geophysical Research Letters, Space Sciences, 37(23),  
438 <https://doi.org/10.1029/2010GL045430>

439

440 Mannucci, A.J., Wilson, B.D., Yuan, D.N., Ho, C.H., Lindqwister, U.J., Runge, T.F. (1998); A  
441 global mapping technique for GPS-derived ionospheric total electron content  
442 measurements. Radio Sci. 33, 565-582, <http://dx.doi.org/10.1029/97RS02707>.

443 Malik, Rakhee, Sarkar, Shivalika, Mukherjee, Shweta, Gwal, A.K (2010); Study of ionospheric  
444 variability during geomagnetic storms. J. Ind. Geophys. Union 14 (1), 47-56.

445 **Misra, P., Enge, P. (2006); Global Positioning System: Signals, Measurements and**  
446 **Performanc 2<sup>nd</sup> ed., Ganga-Jamuna Press, Lincoln, MA01773.**

447 Nahavandchi, H., Soltanpour, A. (2008); Local ionospheric modeling of GPS code and carrier  
448 phase observation, vol. 40,309, pp.271-284.

449 Nigussie, M., Radicella, S.M., Damtie, B., Nava, B., Yizengaw, E., Groves, K. (2013);  
450 Validation of the NeQuick 2 and IRI-2007 models in East-African equatorial region.  
451 J. Atmos. Sol-Terr. Phys., <http://dx.doi.org/10.1016/j.jastp.2013.04.016>.

452 Norsuzila, Y., Ismail, M., Abdullah M. (2008); Investigation of the GPS signals ionospheric

453 correction: Ionospheric TEC prediction over equatorial region, IEEE International  
454 Conference on Telecommunications and Malaysia International Conference on  
455 Communications (ICT-MICC 2007); Penang, Malaysia. 294-298, 14-17.

456 Norsuzila, Y., Mardina, A., Mohamod, I., Azami, Z. (2009); Model validation for Total  
457 electron content (TEC) at equatorial region, European Journal of scientific research vol.28,  
458 No.4, pp 642-648.

459 Olwendo, O.J., Baki, P., Mito, C., Doherty, P. (2012a); Characterization of ionospheric  
460 GPS total electron content (GPS TEC) in low latitude zone over the Kenyan region  
461 during a very low solar activity phase. *J. Atmos. Sol-Terr. Phys.*, 84-85:52-61.

462 Olwendo, O.J., Baki, P., Mito, C., Doherty, O. (2012b); Comparison of GPS TEC variations with  
463 IRI-2007 TEC prediction at equatorial latitudes during a low solar activity (2009-2011)  
464 phase over the Kenyan region. *J Adv Space Res.*  
465 <http://dx.doi.org/10.1016/j.asr.2012.08.001>.

466 Rios, V.H., Medina, C.F., Alvarez, P. (2007); Comparisons between IRI predictions and  
467 digisonde measurements at Tucuman. *J. Atmos. Sol. Terr.* 69, 569-577..

468 Sobral, J. H., M. A. Abdu, C. S. Yamashita, W. D. Gonzalez, A. C. de Gonzalez, I. S. Batista, C.  
469 J. Zamlutti, and B. T. Tsurutani (2001); Responses of the low-latitude ionosphere to very  
470 intense geomagnetic storms, *J. Atmos. Sol. Terr. Phys.*, 63, 965–974, doi:10.1016/S1364  
471 6826(00)00197-8.

472 Sethi, N., Dabas, R., Sarkar, S. (2011); Validation of IRI 2007 against TEC observations during  
473 low solar activity over Indian sector.

474 Tariku Y.A. (2015a); Patterns of GPS-TEC variation over low-latitude region (African sector)  
475 during the deep solar minimum (2008 to 2009) and solar maximum (2012 to 2013) phases.

476 Earth, Planets, Space 67:35. doi:10.1186/ s40623-015-0206-2.

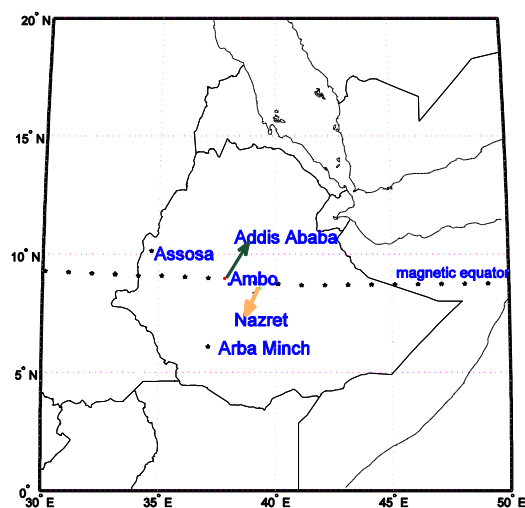
477 Tariku, Y.A. (2015b); TEC prediction performance of the IRI-2012 model over Ethiopia during  
 478 the rising phase of solar cycle 24 (2009-2011), Earth, Planets and Space (2015) 67:140  
 479 DOI 10.1186/s40623-015-0312-1.

480 Tsurutani, B., et al. (2004); Global dayside ionospheric uplift and enhancement associated with  
 481 interplanetary electric fields, J. Geophys. Res., 109, A08302, doi: 10.1029/2003JA010342.

482 Venkatesh, K., P. V. S. Rama Rao, P. L. Saranya, D. S. V. V. D. Prasad, and K. Niranjana (2011);  
 483 Vertical electron density and topside effective scale height (HT) variations over the Indian  
 484 equatorial and low latitude stations, Ann. Geophys., 29, 1861–1872, doi:10.5194/angeo-29-  
 485 1861-2011.

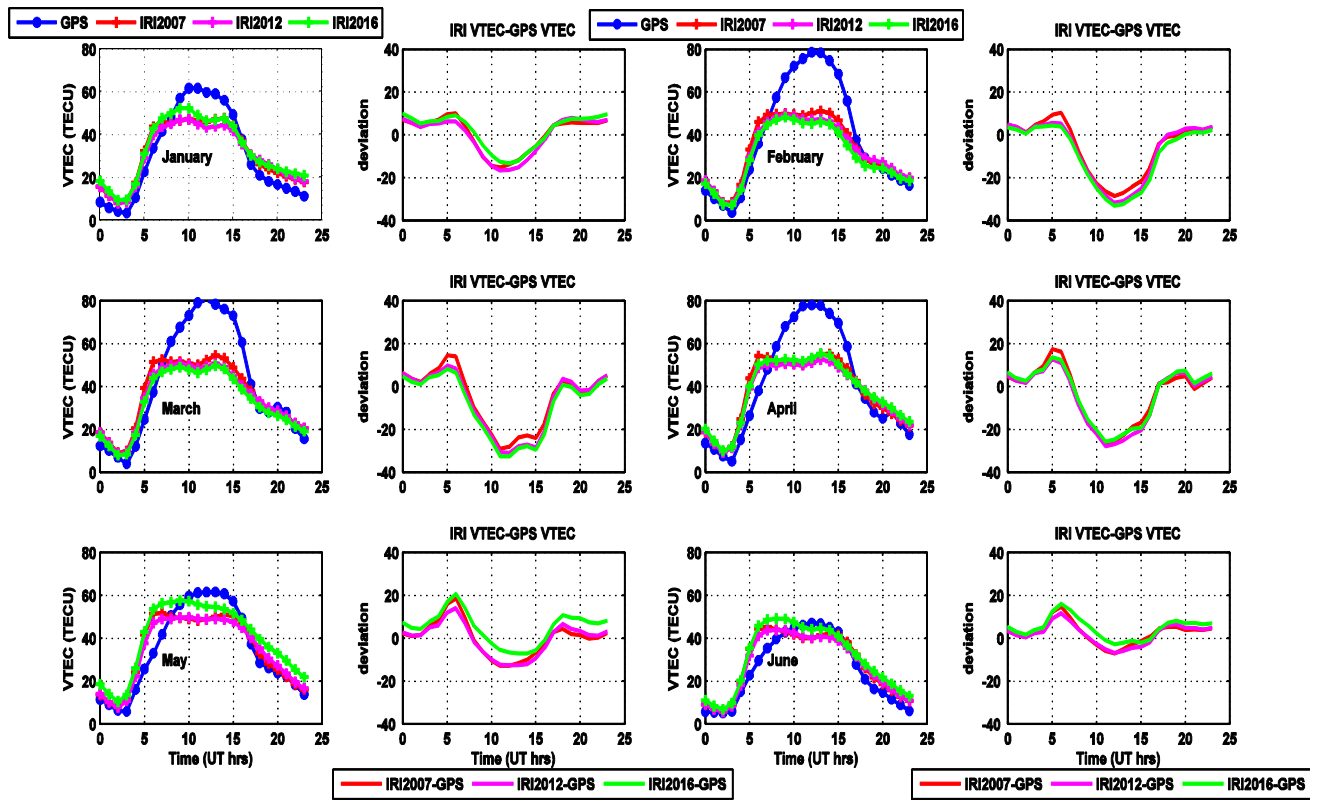
486 Wu, C.C., Fry, C.D., Liu, J.Y., Liou, K., Tseng, C.L. (2004); Annual TEC variation in the  
 487 equatorial anomaly region during the solar minimum: September, 1996-August 1997., J.  
 488 Atmos. Terr. Phys., 66:199-207.

490 Figures



491

492 Figure 1: Location of GPS receivers used for the study

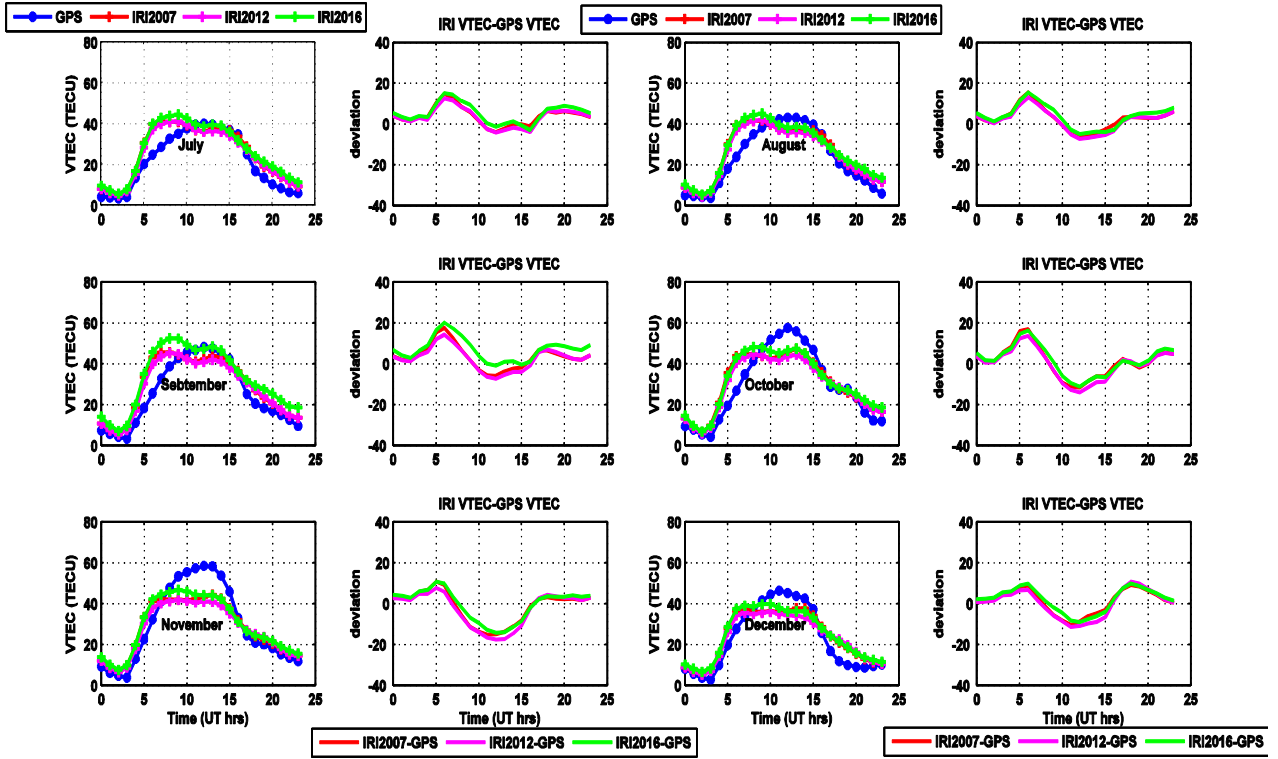


493

494 Figure 2: A graph to illustrate diurnal monthly VTEC variation and performance of the IRI

495 model over Arba Minch station during the period of January-June in 2015

496



497

498 Figure 3: A graph to illustrate diurnal monthly VTEC variation and performance of the IRI

499 model over Arba Minch station during the period of July-December in 2015

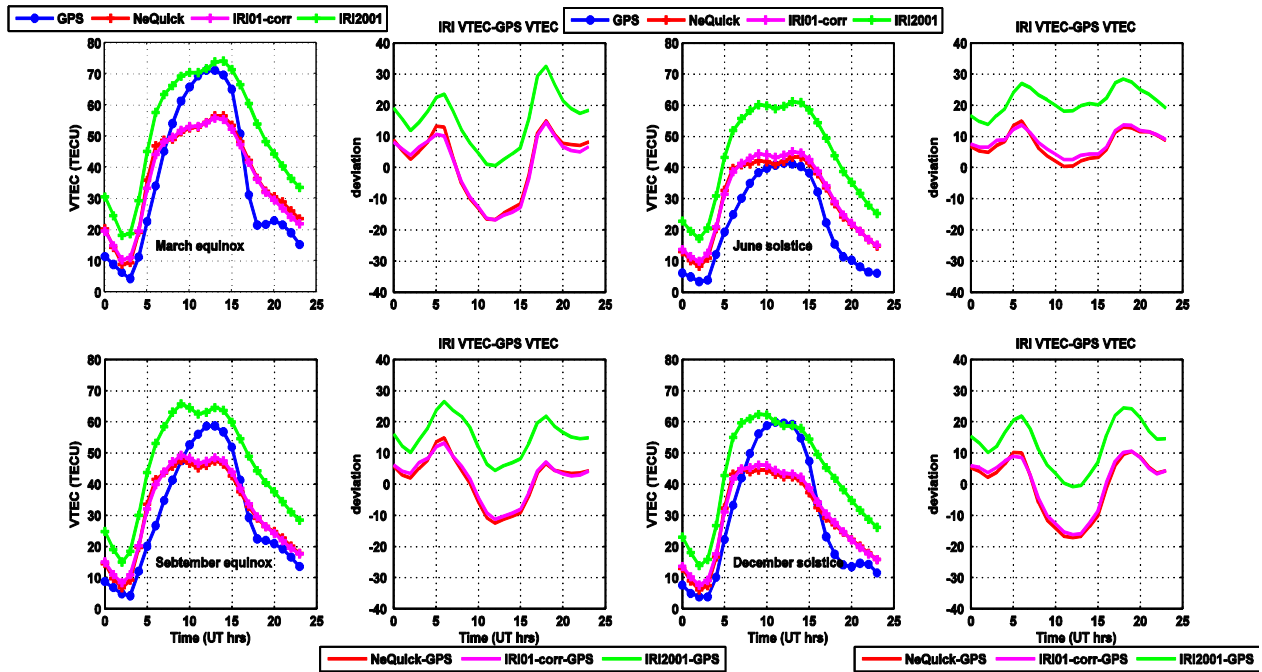


500

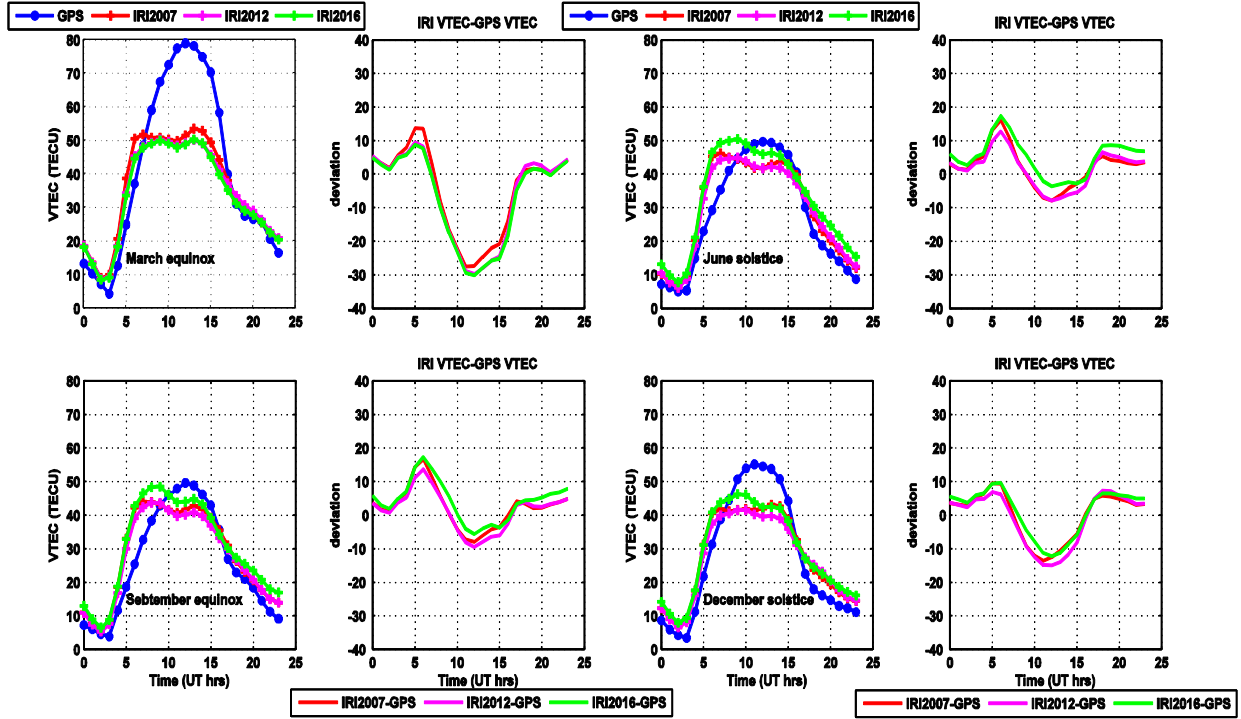
501



502 Figure 4: A graph to illustrate diurnal seasonal VTEC variation and performance of the IRI-2012  
 503 model over Ambo station during the period of 2013



504  
 505 Figure 5: A graph to illustrate diurnal seasonal VTEC variation and performance of the IRI-2012  
 506 model over Ambo station during the period of 2014

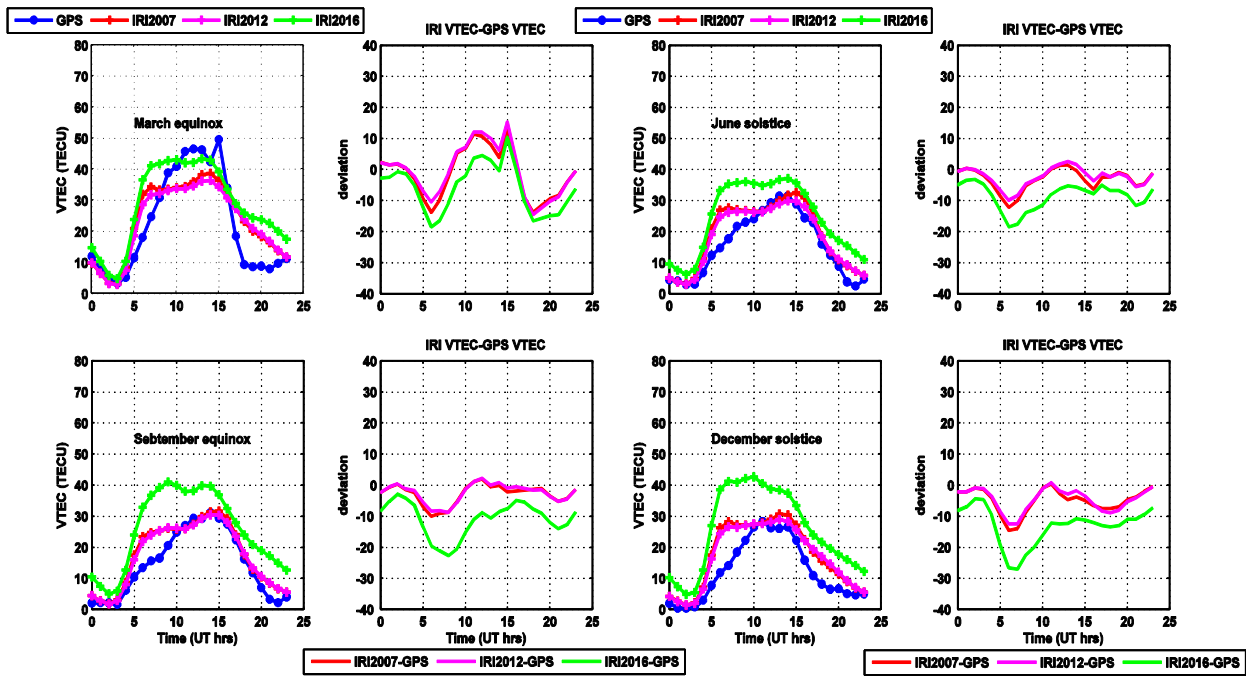


507

508

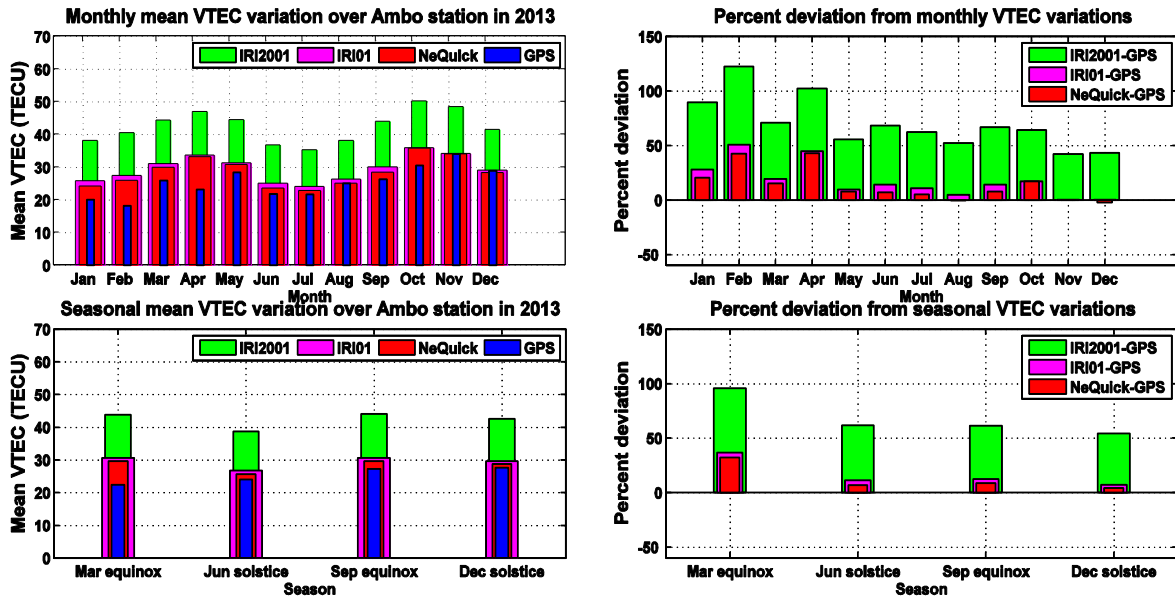
509 Figure 6: A graph to illustrate diurnal seasonal VTEC variation and performance of the IRI

510 model over Arba Minch station during the period of 2015

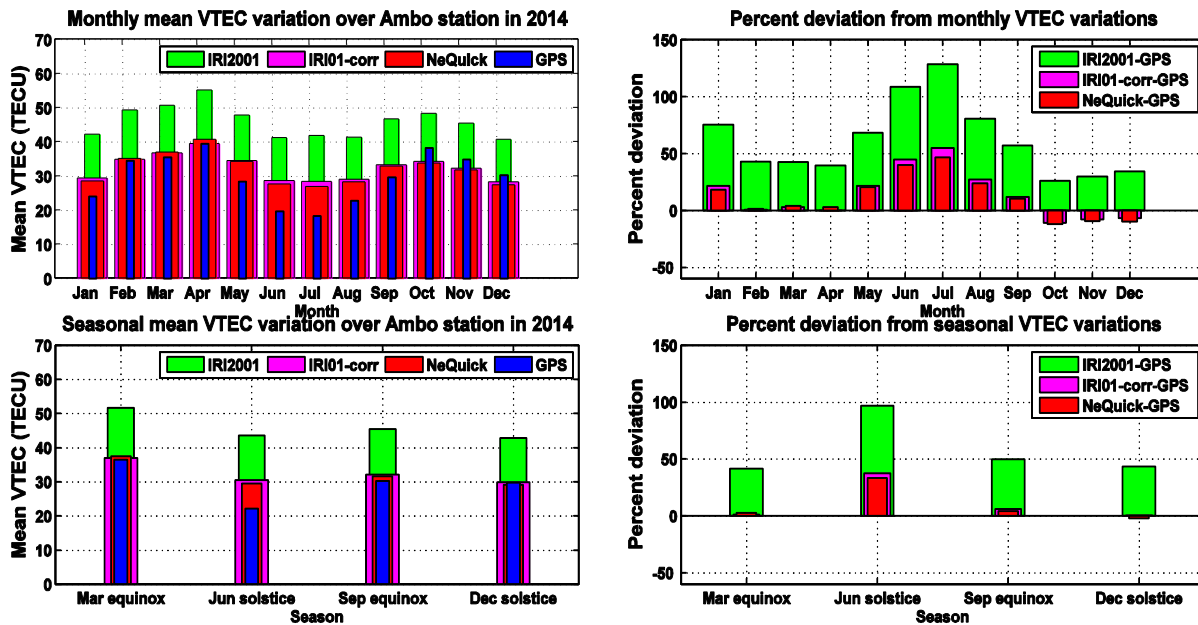


511

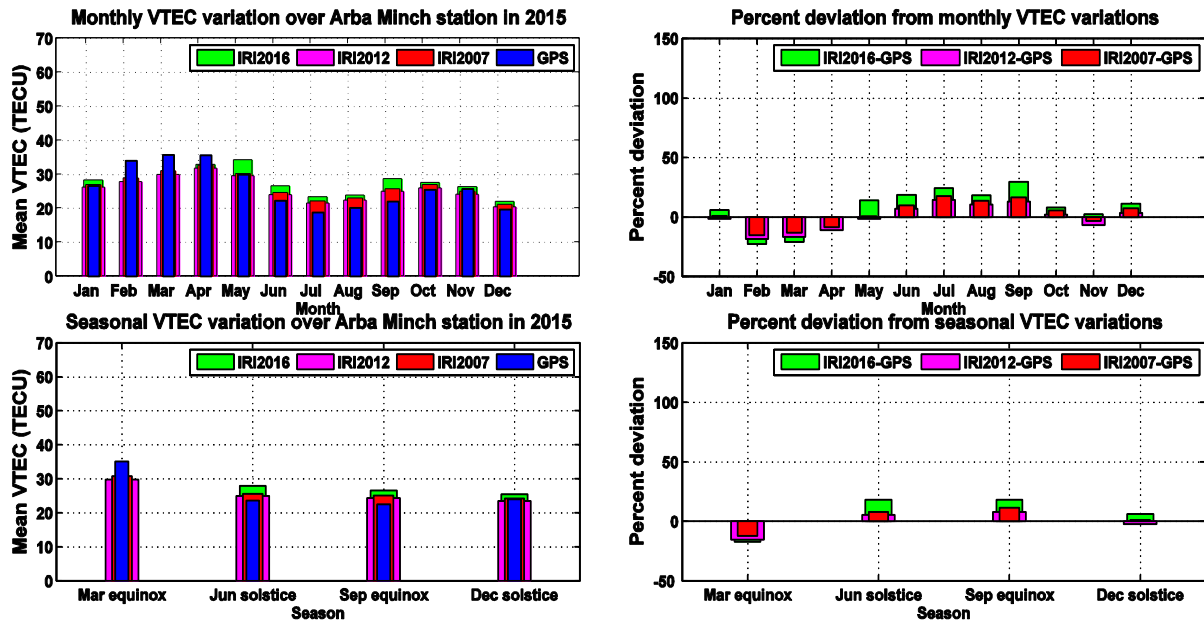
512 Figure 7: A graph to illustrate diurnal seasonal VTEC variation and performance of the IRI  
 513 model over Asosa station during the period of 2016



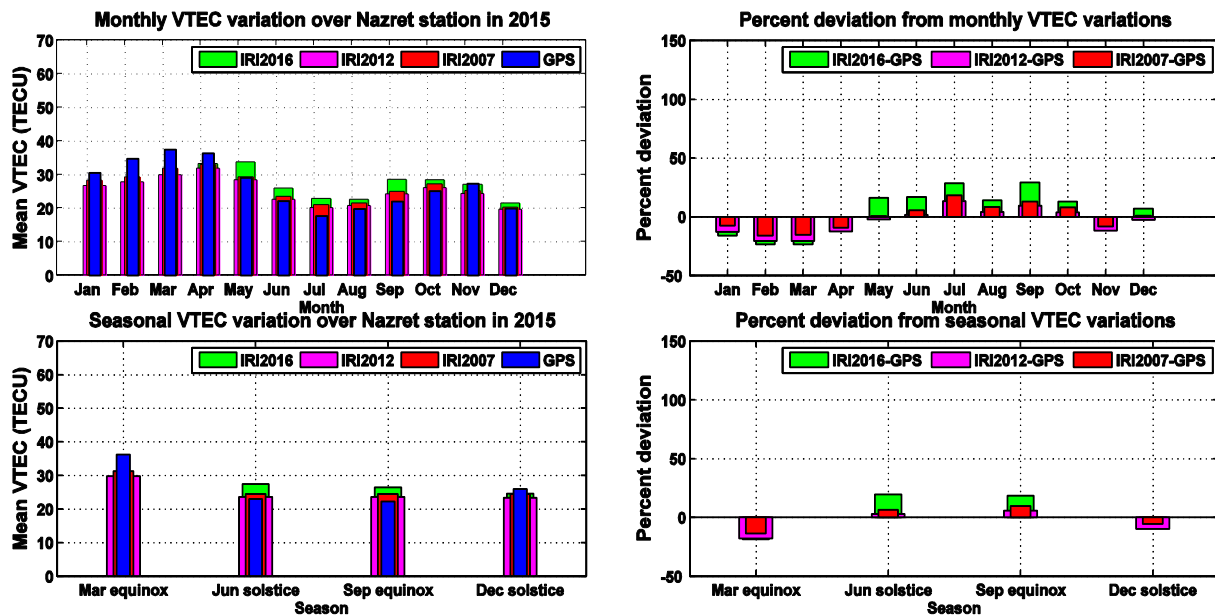
514  
 515 Figure 8: A graph to illustrate the arithmetic mean monthly and seasonal VTEC variation and  
 516 performance of the IRI-2012 model over Ambo station during the period of 2013



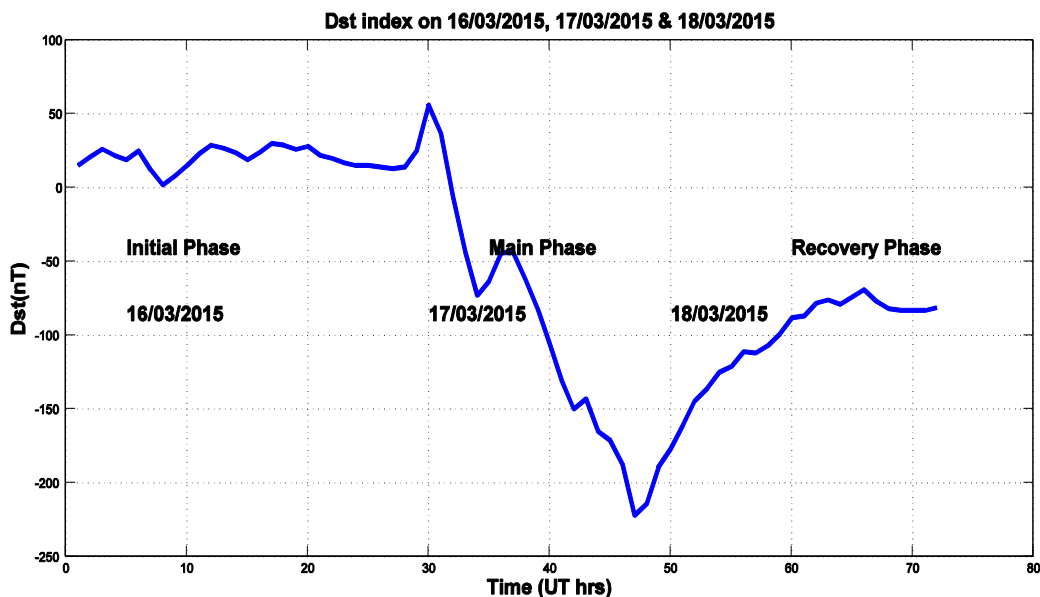
518 Figure 9: A graph to illustrate the arithmetic mean monthly and seasonal VTEC variation and  
 519 performance of the IRI-2012 model over Ambo station during the period of 2014



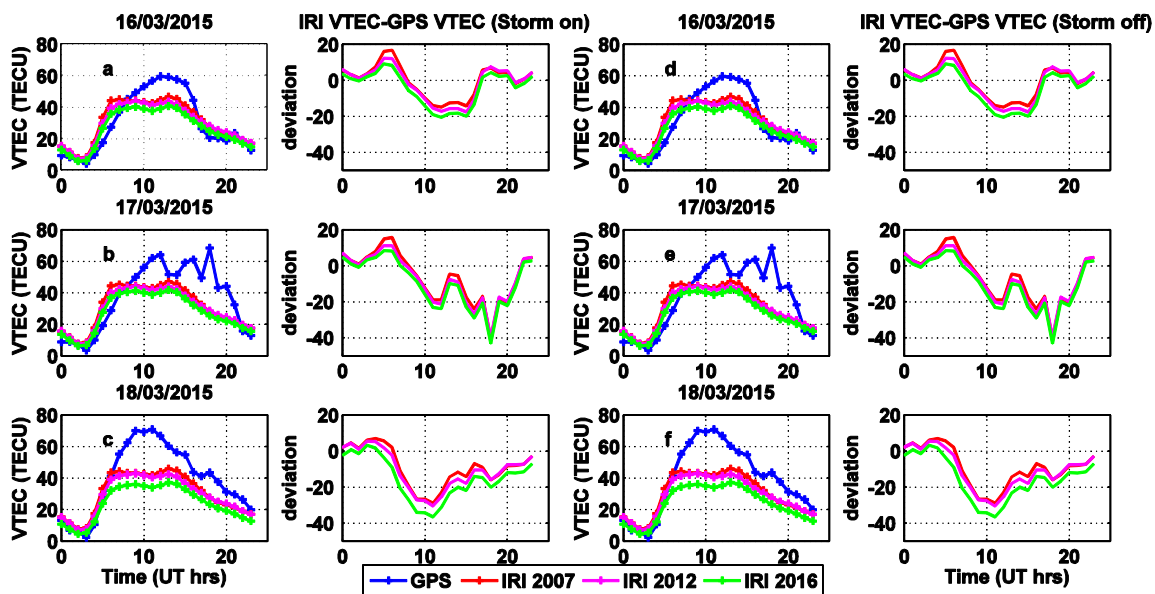
520  
 521  
 522 Figure 10: A graph to illustrate the arithmetic mean monthly and seasonal VTEC variation and  
 523 performance of the IRI model over Arba Minch station during the period of 2015



525 Figure 11: A graph to illustrate the arithmetic mean monthly and seasonal VTEC variation and  
 526 performance of the IRI model over Nazret station during the period of 2015



527  
 528  
 529 Figure 12: Dst index on 16/03/2015, 17/03/2015, and 18/03/2015 as observed over Arba Minch  
 530 station during the period of 2015 (data source for Dst index: World Data Center, Kyoto  
 531 University).



532  
 29

533 Figure 13: A graph to show the variation of the VTEC and the response of IRI model on storm  
 534 time condition which occurred on March 17/2015 as observed over Arba Minch station. Figures  
 535 14a–14c and Figures 14d–14f show patterns of the modeled and measured VTEC values when  
 536 the storm option is “on” and “off,” respectively.

<b>Station</b>	<b>code</b>	<b>Geographic coordinates Lat. (N), Long. (E)</b>	<b>Geomagnetic coordinates Lat. (N), Long. (E)</b>	<b>Dip angle</b>
<b>Asosa</b>	asos	(10.05,34.55)	(0.56,106.38)	3.2
<b>Ambo</b>	aboo	(8.97,37.86)	(0.07,109.80)	1.2
<b>Nazret</b>	nazr	(8.57,39.29)	(-0.08,111.27)	1.19
<b>Arba Minch</b>	armi	(6.06,37.56)	(-3.08,109.57)	-5.7

537  
 538

539 Table 1: Coordinates of GPS receivers used for the study

540